PHYSICAL REVIEW A VOLUME 16, NUMBER 2 AUGUST 1977

Excitation cross sections and polarization of impact radiation in Be^+-Mg^+–He-Ne high-energy collisions: A comparison of model potential calculations

Svend Erik Nielsen
Chemistry Laboratory III, H. C. Ørsted Institute, University of Copenhagen, DK-2100 Copenhagen Ø, Denmark

John S. Dahler
Department of Chemistry, University of Minnesota, Minneapolis, Minnesota 55455
(Received 3 December 1976)

Cross sections and polarization of impact radiation have been calculated for the excitation of $Be^+(2s)$ and $Mg^+(3s)$ ions in collisions with ground-state He and Ne atom targets in the energy range $E_{c.m.} = 0.5$–100 keV. Each ion-atom pair has been treated as a quasi-one-electron three-particle system consisting of the valence electron of the ion, the closed-shell ion core, and the closed-shell rare-gas atom. The interactions among these three have been represented by model potentials. Charge transfer and excitation of the rare-gas target atoms are neglected. We have obtained three- and seven-state (in the case of Mg^+) close-coupling solutions to the impact-parameter equations, assuming a rectilinear trajectory for the motion of the two heavy particles. Comparisons are made of theoretical predictions based on two Bottcher-type model potentials (V_{B1} and V_{B2}) and the simple Hartree-Fock frozen-core potential (V_{HF}) for the electron–rare-gas interaction. The predictions based on V_{HF} agree better with experimental results than do those based on V_{B1} or V_{B2}, especially in the case of Be^+-Mg^+-He collisions.

I. INTRODUCTION

The present investigation is an outgrowth of a recent study[1] where we reported theoretical estimates of the excitation cross sections for high-energy ($0.5 \leq E_{c.m.} \leq 100$ keV) Be^+ and Mg^+ ions in collision with He and Ne atoms. In that earlier investigation we adopted for the interaction between the rare-gas target atom and the valence electron of the ion a model potential V_{B1} proposed by Bottcher *et al.*[2] To estimate the excitation cross sections, we then chose for the electronic basis a finite number of bound states of the alkaline earth ion, and solved numerically the associated set of close-coupled equations in the impact-parameter approximation. Although there was qualitative accord between experimental data (Andersen *et al.*[3]) and our theoretical estimates of the inelastic cross sections and polarization of the impact radiation, the agreement was by no means quantitative. The theory seldom was able to generate accurate estimates of the magnitudes of the cross sections or of the energies at which these cross sections were maximal. Furthermore, the theory invariably predicted that the polarization was more positive at low energies than experiments indicated.

In another recent study[4] we have examined how the theoretical predictions of inelastic scattering cross sections for the neutral quasi-one-electron systems Li-Na–He-Ne depend on the choice of model potential. One important part of this study was a comparison of results based on the fundamentally different Baylis[5] and Bottcher model potentials. Calculations for Li–He-Ne revealed that V_{HF}, a simple Hartree-Fock electrostatic approximation for the electron–rare-gas interaction which completely neglects core distortion, can produce results that compare rather favorably with those based on more sophisticated models. Among these are the Bottcher potentials V_{B1}, which allow for distortion of the rare-gas atom by the electron, and V_{B2}, which also includes the distortion due to the presence of the positively charged projectile ion. The cross sections and polarizations predicted by these two model potentials were found to be distinctly different from those based on V_{HF}, but differed by very little from one another. However, it is reasonable to expect that for the alkaline-earth-ion–rare-gas collisions considered here there will be greater differences between the predictions based on V_{B1} and V_{B2}; the polarizations caused by the Be^{2+} and Mg^{2+} projectile cores are far larger than those induced by Li^+ and Na^+.

Here we shall report the results of calculations for the systems Be^+-Mg^+–He-Ne which were made using (i) V_{B2}, the version of the Bottcher potential which presumably is superior to V_{B1} because it includes the interactions associated with the electron projectile ion "cross polarization," and (ii) the much simpler Hartree-Fock frozen-core potential V_{HF}. For the single system Be^+-He, we also have made calculations based on an earlier version[6] of Bottcher's model potential V_{B1}. Using these various potentials, we generate theoretical

estimates of the cross sections and radiative polarizations associated with the $2s \rightarrow 2p$ transition of Be^+ and with the $3s \rightarrow 3p, 3d, 4s$ excitations of Mg^+. These results then are compared with our earlier predictions based upon V_{B1} and with the available experimental data.[3,7]

Here, just as before, we use the semiclassical impact parameter method and select rectilinear constant-velocity trajectories. The wave function of the valence electron is represented by a linear combination of a finite number of pseudo-one-electron states of the projectile ion. Thus, we ignore both charge exchange and excitation of the target gas. The rationale for this is the experimental observation that throughout the medium-to-high energy range $E_{c.m.} \approx 1$–100 keV, the projectile resonance transition ($2s \rightarrow 2p$ for Be^+, $3s \rightarrow 3p$ for Mg^+) dominates by an order of magnitude all other direct excitations and charge-transfer events. The exception to this is the quasihomonuclear system Mg^+-Ne for which, at impact energies less than 10 keV, charge transfer and target excitation compete favorably with projectile excitation.[8]

Most previous theoretical studies of excitation in ion-atom collisions have dealt with symmetric or nearly symmetric systems such as H^+-H,[9] Li^+-Li,[10] or Li^+-Na.[11–13] For cases such as these, charge-transfer channels play very important roles and, indeed, the cross sections for charge exchange often have been the principal objectives of these earlier investigations. Furthermore, for these symmetric systems it seems most natural to adopt a molecular representation for the electronic state. In contrast to this, the systems which concern us here are grossly asymmetric and experiments show that the collisions rarely result in charge transfer or target excitation. Therefore, it is reasonable to adopt, as a first-order approximation, an expansion of the electronic wave function in terms of atomic states of the projectile ion. The adequacy of this approximation is by no means certain, the only sure test being to examine (as we now are preparing to do) the consequences of extending the basis to include charge transfer and target excitation channels. There are a few previous studies of asymmetric systems, particularly for the excitation of H by He (Refs. 14–16) in collisions of moderate energy, which lend support to the single-center approximation, but similarly constructed estimates of the excitation cross sections of H in medium-energy collisions with the heavier rare gases Ne, Ar, and Kr[17] exceed experimental observations by as much as an order of magnitude. At low energies, expansions in terms of molecular two-center states are likely to converge more rapidly and to be more susceptible to conventional interpretation than are expansions in terms of atomic states. In recent calculations for the system H-He, Bell *et al.*[18] and Benoit and Gauyacq[19] obtained very good agreement with low-energy experiments for the $2s \rightarrow 2p$ total excitation cross section by invoking the Coriolis coupling between the $^2\Sigma$ and $^2\Pi$ molecular states. The way in which these calculations were done did, however, preclude the possibility of constructing a physically meaningful estimate for the polarization of the impact radiation.

In addition to our previous investigations[1,4] of the excitation of pseudo-one-electron atoms and ions due to collisions with rare gas atoms, the Bottcher model potentials have been used in a number of other atomic collision problems. These include theoretical estimates of collisional line broadening[2] and of collision-induced absorption and fine-structure transitions,[20] the collisional quenching of metastable hydrogen atoms,[21] and the charge-transfer cross section for Na^+-Li.[22]

II. THEORY

A. Model Hamiltonians

We shall treat the colliding rare-gas atom (He or Ne) and alkaline-earth ion (Be^+ or Mg^+) as a quasi-one-electron system. The interactions among the valence electron of the projectile ion and the closed-shell cores of the ion A (Be^{2+} or Mg^{2+}) and rare-gas target atom B are represented by models for the e-A, e-B, and A-B potentials; cf. Fig. 1. For the first of these we select an effective-charge Coulomb potential (atomic units $e = m_e = \hbar = 1$ being used throughout)

$$V_A(r_1) = -Z_{\text{eff}}(r_1)/r_1 = -[(Z_N - Z_A)/r_1]\, e^{-r_1/\alpha}(1 + r_1/2\alpha) - Z_A/r_1 , \tag{1}$$

that is characteristic of the isolated projectile ion, Be^+ or Mg^+. Here $Z_A = +2$ is the charge of the

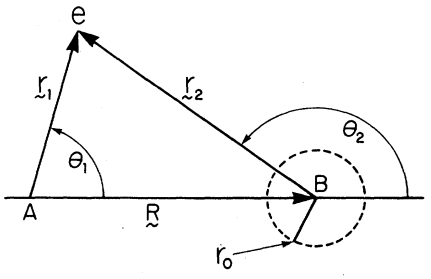

FIG. 1. Coordinates used to describe the relative positions of the closed-shell projectile ion core A (Be^{++} or Mg^{++}), the valence electron e, and the closed-shell target atom B (He or Ne). The radius r_0 indicates a cutoff radius for the long-range induced e-B interactions, cf. Eqs. (7)–(9).

projectile core and Z_N is that of the bare projectile nucleus. The value of the parameter α is chosen so that the eigenvalue of the one-electron Hamiltonian operator

$$H_A = -\tfrac{1}{2}\nabla_{r_1}^2 + V_A(r_1) \ , \tag{2}$$

which corresponds to the ground state of the projectile ion ($2s$ state of Be^+, $3s$ state of Mg^+) will equal the observed ionization potential. The spectrum of the operator H_A generated by this procedure is in fair agreement with experiment.[1]

The Hamiltonian for the valence electron in the field of the two closed-shell cores may be written

$$H = H_A(\vec{r}_1) + V_I(\vec{r}_2, \vec{R}) \ , \tag{3}$$

$$V_I(\vec{r}_2, \vec{R}) = U_e(\vec{r}_2, \vec{R}) + W_{AB}(R) \ , \tag{4}$$

where we have separated from the total interaction V_I that part $W_{AB}(R)$ which is independent of the electron coordinate. W_{AB} may include a short-range core-core interaction and a long-range monopole-induced dipole potential as well. Because it depends solely upon the core-core separation R this part of the total interaction contributes only to the differential cross sections and not to total inelastic cross sections.[1]

The purpose of this study is to compare theoretical predictions of collision cross sections based on three different choices for the interaction $U_e(\vec{r}_2, \vec{R})$, all of which are related to model potentials of Bottcher.[2,6] The simplest of these is to adopt for U_e the electrostatic interaction between the valence electron and the charge distribution characteristic of the undistorted ground state of the rare-gas atom. To represent this charge distribution we use the Hartree-Fock self-consistent-field (SCF) orbitals $\chi_{nlm}(\vec{r}) = R_{nl}(r)Y_{lm}(\hat{r})$, as tabulated by Clementi,[23] and so obtain for the electrostatic interaction the formula

$$\begin{aligned} V_{\rm HF}(r) &= \langle \Phi_0 | \sum_{j=1}^{N} \frac{1}{|\vec{r} - \vec{r}_j|} | \Phi_0 \rangle - \frac{N}{r} \\ &= 2\sum_{nlm} \int d^3r' \, \frac{|\chi_{nlm}(\vec{r}')|^2}{|\vec{r} - \vec{r}'|} - 2\sum_{nl} \frac{2l+1}{r} \\ &= -\frac{2}{r}\sum_{nl}(2l+1)\int_r^\infty dr' \, r'^2 R_{nl}^2(r')\left(1 - \frac{r}{r'}\right) \ , \end{aligned} \tag{5}$$

where Φ_0 is the Hartree-Fock wave function for the closed-shell ground state of the N-electron rare-gas atom. Most theoretical studies of H rare-gas collisions have made use of potentials of this sort.[14-17]

The identification of U_e with $V_{\rm HF}$ amounts to a total neglect of the distortions of the rare-gas target atom due to the presence of the electron and of the projectile core A. In an effort to remedy these defects of the Hartree-Fock model, Bottcher[6] and Bottcher *et al.*[2] proposed the modification

$$\begin{aligned} V_{B1}(r_2) = V_{\rm HF}(r_2) &- \frac{\alpha_d}{2r_2^4} w_6(r_2) - \frac{\alpha_q'}{2r_2^6} w_8(r_2) \\ &+ (c_0 + c_1 r_2 + c_2 r_2^2)\exp\left(\frac{-r_2}{r_0}\right) \ , \end{aligned} \tag{6}$$

the last term of which is a short-range potential with parameters c_n and r_0 so chosen that V_{B1} will reproduce the experimental momentum-transfer cross sections for e rare-gas collisions over a wide range of energies. The second and third terms of V_{B1} represent the long-range interactions between the electron and the induced dipole and quadrupole moments of the rare-gas atom. The purpose of the functions $w_n(r_2)$ is to remove the strong singularities of these multipole interactions. In Bottcher's original (1971) presentation these cutoff functions were chosen to be of the form[6]

$$w_n^1(r_2) = 1 - \exp[-(r_2/r_0)^n] \ , \tag{7}$$

with $r_0 = 0.355$ a.u. for He and $r_0 = 0.90$ a.u. for Ne. We label this version of the Bottcher potential V_{B1}^1. A later version (1973) used the much softer cutoff functions[2]

$$w_n(r_2) = 1 - \left(\sum_{t=1}^{n} \frac{(r_2/r_0)^{t-1}}{(t-1)!}\right)\exp\left(\frac{-r_2}{r_0}\right) \ , \tag{8}$$

(with r_0 equal to 0.35 and 0.90 a.u. for He and Ne, respectively) together with a very different set of the short-range potential parameters c_n, cf. Eq. (6). The reason given by Bottcher for replacing the cutoff functions given by Eq. (7) with those of (8) was that this simplified the task of evaluating various molecular integrals which entered into his calculations. In our previously reported applications of Bottcher's model potentials, we always have used the 1973 version of V_{B1} and we do so here as well except in the case of Be^+-He for which calculations based upon V_{B1}^1 also will be reported.

The model potentials V_{B1} (and V_{B1}^1 also) fail to take into account the polarization of the rare-gas atom by the doubly charged projectile core A (Be^{2+} or Mg^{2+}). To account for this Bottcher *et al.*[2] introduced the additional interaction

$$V_{\rm core}(\vec{r}_2, \vec{R}) = V_{ec}(\vec{r}_2, \vec{R}) w_4(r_2) \ , \tag{9}$$

with

$$V_{ec}(\vec{r}_2, \vec{R}) = -\frac{\alpha_d Z_A}{R^2 r_2^2}\cos(\hat{r}_2 \cdot \hat{R}) \ . \tag{10}$$

The potential V_{ec} appears as a cross term when one computes the interaction energy

$$F(\vec{r}_2,\vec{R}) = -\tfrac{1}{2}\alpha_d[Z_A\vec{R}/R^3+\vec{r}_2/r_2^3]^2$$
$$= V_e(r_2)+V_{ec}(\vec{r}_2,\vec{R})+V_c(R)\,, \qquad (11)$$

associated with the polarization of the rare-gas atom by the combined actions of the two monopoles e and A (with charges -1 and $Z_A=+2$, respectively) located at $\vec{r}_2$ and $-\vec{R}$, as depicted in Fig. 1. These same three terms occur in the Baylis model potentials[5] for alkali–rare-gas interactions and recently have been discussed by Wahlstrand *et al.*[24]

The core-core polarization potential $V_c(R)$ can be incorporated within $W_{AB}(R)$ of Eq. (4) and $V_e(\vec{r}_2)$ already appears as the second term of the model potential V_{B1} defined by Eq. (6). We note that when V_{ec} and V_e are incorporated into the Bottcher potentials, each is multiplied by a cutoff function $w_n(r_2)$ which removes the singularity at $r_2=0$. However, the singularities of V_{ec} and W_{AB} at $R=0$ are not treated in this way.

The function

$$V_{B2}(\vec{r}_2,\vec{R}) = V_{B1}(\vec{r}_2,\vec{R})+V_{ec}(\vec{r}_2,\vec{R})w_4(r_2) \qquad (12)$$

is presumably a more realistic estimate of the interaction U_e than V_{B1}. Certainly by including V_e and V_{ec} in the model potential, one is assured that he will get the correct asymptotic limit $V_I \to -\alpha_d(Z_A-1)/R^4$ for the projectile-target interaction. Because of the greater charge of the projectile core (Be^{2+} or Mg^{2+}), it is reasonable to expect that the cross-polarization potential V_{ec} will be more important here than it was in our previously reported study of alkali-metal–rare-gas collisions.[4]

In summary, the four model potentials for which we shall make comparative calculations of inelastic-collision cross sections are the following:

$$U_e^{(1)} = V_{\rm HF}(r_2)\,, \qquad (13)$$

$$U_e^{(2)} = V_{B1}(r_2) = \{V_{\rm HF}+V_{\rm sr}\}+V_e w_6+V_q w_8\,, \qquad (14)$$

$$U_e^{(3)} = V_{B1}^1(r_2) = \{V_{\rm HF}+V_{\rm sr}^1\}+V_e w_6^1+V_q w_8^1\,, \qquad (15)$$

$$U_e^{(4)} = V_{B2}(\vec{r}_2,\vec{R}) = V_{B1}(r_2)+V_{ec}(\vec{r}_2,\vec{R})w_4\,. \qquad (16)$$

Here V_q is the quadrupolar term and $V_{\rm sr}$ is the short-range part of the Bottcher potential given explicitly by the last term of Eq. (6).

B. Scattering equations

It is assumed that the relative motion of the two heavy particles A and B can be described approximately by the rectilinear constant-velocity trajectory $\vec{R}(t) = -\vec{b}-\vec{v}t$ $(-\infty<t<+\infty)$. Here $\vec{b}$ denotes the impact parameter and $\vec{v}$ is the constant velocity associated with the center-of-mass kinetic energy $E_{\rm c.m.}=\frac{1}{2}\mu v^2$, $\mu = M_AM_B/(M_A+M_B)$. To determine the consequences of a collision we must solve the time-dependent Schrödinger equation

$$(i\partial_t - H_{el})\psi(\vec{r}_1,t) = 0\,, \qquad (17)$$

$$H_{el} = H_A(\vec{r}_1)+U_e(\vec{r}_2,\vec{R})\,, \qquad (18)$$

subject to the initial condition

$$\psi(\vec{r}_1,t=-\infty) = \phi^A_{n_0 00}(\vec{r}_1)\exp(-i\epsilon_{n_0 0}t)\,.$$

We choose as a trial function the single-center expansion

$$\psi(\vec{r}_1,t) = \sum_j a_j(t)\phi_j(\vec{r}_1)\exp(-i\epsilon_j t) \qquad (19)$$

in terms of a finite number of the eigenfunctions $\phi_j^A(\vec{r}_1)$ of the projectile Hamiltonian H_A. As a matter of convenience, we have discarded from Eqs. (17) and (18) that part $W_{AB}(R)$ of the potential energy which depends only upon the A-B separation R. The wave function associated with the complete Hamiltonian $H = H_{el}+W_{AB}(R)$ is obtained from (19) by multiplying each amplitude a_j with the corresponding phase factor

$$\exp\left(-i\int_{-\infty}^{t} dt'\,W_{AB}(\vec{R}(t'))\right)\,.$$

These factors contribute nothing to the total inelastic cross sections but they are important to the calculation of differential cross sections.

The amplitudes a_j of Eq. (19) are the solutions of the coupled equations

$$i\dot{a}_j = \sum_{j'} G_{jj'}(t)\exp[i(\epsilon_j-\epsilon_{j'})t]a_{j'} \qquad (20)$$

which satisfy the initial conditions $a_j(t=-\infty) = \delta_{jj_0}$, $j_0=(n_0 00)$. Here $G_{jj'}$ denotes a matrix element of the operator $H_{el}-i\partial_t$.

In our earlier study[1] of Be^+-Mg^+-He-Ne collisions we selected an expansion of $\psi(\vec{r}_1,t)$ in terms of atomic eigenstates $\phi_j^A(\vec{r}_1')$ which were space quantized with respect to the body-fixed rotating frame of reference with the polar axis in the direction $\hat{z}'=\hat{R}$. In this case, the matrix elements $G_{jj'}$ of Eqs. (20) are of the form

$$G_{jj'}^{\rm body} = (vb/R^2)\langle\phi_j^A|\hat{l}_A'|\phi_{j'}^A\rangle+\langle\phi_j^A|U_e|\phi_{j'}^A\rangle$$
$$\equiv C_{jj'}(R)+U_{jj'}^{\rm body}(R)\,, \qquad (21)$$

where $\hat{l}_A'$ is the component of the electronic angular momentum operator perpendicular to the collision plane. The matrix $U_{jj'}^{\rm body}(R) = \delta_{mm'}U_{nlm,n'l'm}$ only connects states with equal magnetic quantum numbers, whereas $C_{jj'}(R) = \delta_{m,m'\pm1}\delta_{nn'}\delta_{ll'}C_{lm,lm'}$ only couples states which belong to the same $(2l+1)$-dimensional manifold.

Because of the long range of the Coriolis couplings $C_{jj'}$, there is an advantage to adopting in Eq. (19) basis functions $\phi_j^A(\vec{r}_1)$ which are space-quant-

ized with respect to the laboratory-fixed frame of reference [with polar axis in the direction of $\hat{z}=\hat{v}=\hat{R}(t=-\infty)$]. For this choice of basis all of the matrix elements $G_{jj'}$ are short-ranged functions of R. These are related to the matrix elements in the body-fixed basis by the formulas

$$G^{\rm lab}_{jj'}(\vec{\mathbf{R}}) = \langle \phi^A_j | U_e | \phi^A_{j'} \rangle \equiv U^{\rm lab}_{jj'}(\vec{\mathbf{R}}) = \sum_\mu R^{(l)}_{m\mu}(\hat{R}) \bar{R}^{(l')}_{m'\mu}(\hat{R}) U^{\rm body}_{nl\mu,n'l'\mu}(R) \ , \qquad (22)$$

where $R^{(l)}_{mm'}(\hat{R})$ denotes a representation coefficient of the rotation group.[25]

Here we solve the close-coupled equations (20) appropriate to the lab-fixed frame of reference. The amplitudes obtained in this way are trivially related to those associated with the body-fixed basis, e.g., in the final state $(t=+\infty)$,

$$a^{\rm lab}_{nlm}(t=+\infty) = e^{-im\Phi}(-)^{l+m} a^{\rm body}_{nl-m}(t=+\infty) \ , \qquad (23)$$

where Φ is the (constant) polar angle of the collision plane.

It is worthwhile to mention that the optimal procedure (in terms of computer time) for solving the close-coupled equations (20) for an initial s state is to use the body-fixed representation Eq. (21), limit the trajectory integration to a finite range $z_{\rm in} \leq z \leq z_{\rm fin}$ $(z=vt)$ determined solely by the range of $U^{\rm body}_{jj'}(R)$, and obtain the final $(t=+\infty)$ amplitudes, say $a^{\rm lab}_{nlm}(+\infty)$, from the amplitudes $a^{\rm body}_{nlm}(z_{\rm fin})$ by using the relationship

$$a^{\rm lab}_{nlm}(+\infty) \simeq a^{\rm lab}_{nlm}(z_{\rm fin}) = e^{-im\Phi} \sum_{m'} r^{(l)}_{mm'}(\theta) a^{\rm body}_{nlm'}(z_{\rm fin}) \ . \qquad (24)$$

Here $\theta = \arccos[-z(b^2+z^2)^{-1/2}]$ and $r^{(l)}_{mm'}(\theta)$ is one of the real-valued matrix elements of the rotation operator.[25] A further discussion of the choice of basis and of its computational aspects can be found in Ref. 4.

C. Matrix elements

Before comparing scattering predictions based on the different model potentials it is useful to examine the relevant matrix elements of these potentials. Techniques for evaluating these matrix elements have been described previously.[1,24]

In Figs. 2(a) and 2(b) we present the off-diagonal matrix elements $U^{\rm body}_{2s,2p_0}$ for Be^+-He and $U^{\rm body}_{3s,3p_0}$ for Mg^+-He. In Figs. 2(c) and 2(d) are plotted the corresponding matrix elements for Be^+-Ne and Mg^+-Ne, respectively. In each case results are given for the three model potentials $V_{\rm HF}$, V_{B1}, and V_{B2}. The values of these matrix elements indicate the degree of coupling between the initial s states and those excited states which are known from experiments to be the most likely products of collisions at the impact energies of interest to us here. We have chosen to plot $R^2U_{12}(R)$ because V_{B2} diverges as R^{-2} at $R=0$.

One sees from these plots that the Hartree-Fock electrostatic potential $V_{\rm HF}$ produces matrix elements of shorter range and considerably smaller magnitudes than does either V_{B1} or V_{B2}. This is especially pronounced when He is the target atom.

The model potential V^1_{B1} (the original 1971 version of Bottcher[6]) has been studied only for Be^+-He. The result for $U^{\rm body}_{2s,2p_0}$, included in Fig. 2(a), is shaped much like that predicted by V_{B1}, but is about 20 times larger. The cause of this extraordinary behavior is the set of cutoff functions $w^1_n(r_2)$ which are found to produce very strong induced interactions for values of r_2 comparable to r_0. It also should be noted that the c^1_n parameters of V^1_{B1}, obtained from fitting theoretical predictions to experimental momentum-transfer cross sections for e-He, are quite different from those of V_{B1}.

The matrix elements of the two Bottcher-type potentials V_{B1} and V_{B2} do, of course, differ dramatically for values of R less than about 1 a.u. Furthermore, there are noticeable differences at intermediate to large values of R where the effect of V_{ec} is to counteract the long-range electron-induction potential V_e. These differences are much greater for Be^+-Mg^+-He than for Be^+-Mg^+-Ne because the Ne interactions are so strongly dominated by the $V_{\rm HF}$ parts of the Bottcher potentials. Comparison with our previous V_{B1} and V_{B2} calculations of off-diagonal matrix elements for Li-Na-He-Ne (for which $Z_A=1$) [Figs. 3(d) and 4(d) of Ref. 20], reveals that cross polarization has a significantly stronger effect here where $Z_A=2$.

III. EXCITATION CROSS SECTIONS

The integral cross section for the transition $j_0(=n_000) \to j(=nlm)$ is related to the solutions $a_j(t)$ of the close-coupled equations (20) by the formula

$$\sigma_{nlm}(E) = 2\pi \int_0^\infty db\, b\, |a_{nlm}(b,E,t=+\infty)|^2 \ . \qquad (25)$$

However, in place of these cross sections, which are specific to the individual magnetic substates, we concern ourselves here with the sum

$$\sigma_{nl}(E) = \sum_m \sigma_{nlm}(E) \ , \qquad (26)$$

over the entire $(2l+1)$-dimensional manifold of magnetic substates belonging to the term (nl).

We have computed the amplitudes a_{nlm} for Be^+-

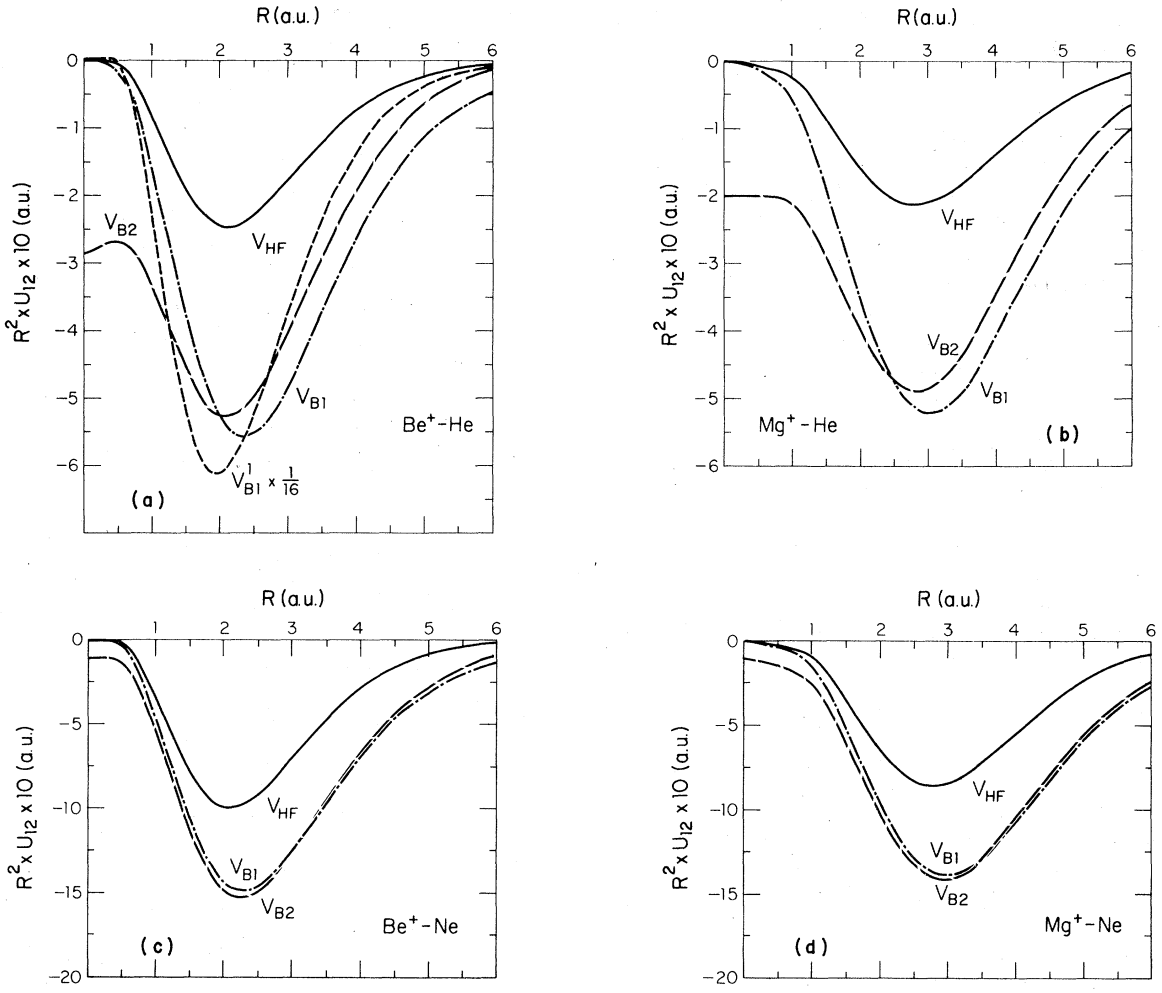

FIG. 2. Off-diagonal matrix elements $U_{12}^{\text{body}}(R)$ based on the model potentials V_{B1}, V_{B2}, and V_{HF}, Eqs. (14)–(17), for the $(n_0 00 \rightarrow n_0 10)$ transition of the ion projectile in (a) Be^+-He, (b) Mg^+-He, (c) Be^+-Ne, and (d) Mg^+-Ne collisions (n_0 equals 2 and 3 for Be^+ and Mg^+, respectively). Note that $R^2U_{12}(R)$ has been plotted against R, the internuclear distance.

He-Ne collisions from the close-coupled equations for the three states $2s$, $2p_0$, and $2p_1$ (or $2p_{-1}$). For Mg^+–He-Ne we have solved the three-state ($3s$, $3p_0$, $3p_1$ or $3p_{-1}$) and the seven-state ($3s$, $3p_0$, $3p_1$ or $3p_{-1}$, $3d_0$, $3d_1$ or $3d_{-1}$, $3d_2$ or $3d_{-2}$, $4s$) equations as well. Some of our results for the model potential V_{B1} were reported previously.[1]

To provide checks on our programs for evaluating matrix elements and solving the scattering equations we performed four-state ($1s$, $2s$, $2p_0$, $2p_1$ or $2p_{-1}$) close-coupling calculations for H–He-Ne collisions using the Hartree-Fock electrostatic potential V_{HF}. Our results for the $1s \rightarrow 2s$ and $1s \rightarrow 2p$ excitation cross sections agreed very well with previous closely analogous calculations of Flannery[14] and of Levy.[17]

A. Be^+-He

In Fig. 3 we display (on a log-log plot) the $2s \rightarrow 2p$ excitation cross section for Be^+-He collisions. The results presented here were obtained from three-state close-coupling calculations based on the model potentials V_{HF}, V_{B1}, V_{B1}^1, and V_{B2}. Shown also is the experimental 2^2S-2^2P multiplet emission cross section obtained by Andersen *et al.*[3] According to their estimates the contribution from cascading is significant only for energies beyond the emission maximum, rising to about 30% at $E_{\text{c.m.}} \simeq 20$ keV.

As we would expect from the discussion of Sec. II C, the predictions of the model potential V_{B2} differ from those of the simpler potential V_{B1}; the

cross-section maximum for V_{B2} is smaller by about 16% and the curve has a somewhat broader shape. However, both V_{B1} and V_{B2} predict that the maximum occurs at an energy of about $E_{\text{c.m.}} \approx 6$ keV which is far greater than the experimental value of $E_{\text{c.m.}} \approx 2.7$ keV. Furthermore, the halfwidth predicted by V_{B2} is quite a bit larger than that observed experimentally.

The cross section predicted by the model potential V_{B1}^{l} does not resemble the experimental result and is greater by a factor of 1.8 or more than that associated with V_{B1}. It is virtually constant over nearly a decade of energy. This same potential has been used to estimate the rate at which collisions with He quench metastable H.[21] The cross section predicted for the $2s \rightarrow 2p$ transition was found to be rather large and nearly independent of energy over the range of energy extending from 0.25 to 10 keV. Although these theoretical predictions match fairly well experimental measurements of the total quenching rate, this agreement is probably fortuitous. Indeed, we believe that the energy independence of the theoretical estimate for the $2s \rightarrow 2p$ cross section is an artifact of the unrealistic potential V_{B1}^{l} and that the near constancy of the experimental quenching cross section should be attributed to the increasing importance at high energies of processes $2s \rightarrow nl(n>2)$ which were not included in the calculations cited above. To partially test this conjecture we performed close-coupling calculations (unpublished) for H(2s)-He collisions and found, just as we had for excitation, that V_{B1}^{l} for $E_{\text{c.m.}} > 1$ keV generates considerably larger and much less energy-dependent cross sections than does V_{B1}. To us it seems an inescapable conclusion that the potential V_{B1}^{l} is unreliable for use in high-energy collisions.

From Fig. 3 we see that the very simple electrostatic potential V_{HF} produces a cross section that agrees extraordinarily well with the experimental results (reportedly good to within 40%). In this case the positions of the theoretical and experimental maxima are identical and the predicted magnitudes lie within the range of experimental uncertainty from 1 to 20 keV. As the energy decreases beyond $E_{\text{c.m.}} = 1$ keV, the cross section predictions based on V_{HF} fall further and further below the experimental values.

B. Mg^{+}-He

Figure 4 shows the $3s \rightarrow 3p$ excitation cross sections for Mg^{+}-He collisions based on the two model potentials V_{B1} and V_{HF} and computed from solutions of the three-state and seven-state close-coupled equations. Shown also is the emission cross section for the 3^2S-3^2P MgII multiplet, corrected for cascading from the 3^2D and 4^2S states. Andersen and his coworkers[3] have estimated that cascading contributions from higher-lying terms of the ^2D and ^2S Rydberg series amount to less than 5% at $E_{\text{c.m.}} = 5$ keV. Therefore, the cascade-corrected 3^2S-3^2P emission cross section presented here should be a good approximation to the $3s \rightarrow 3p$ excitation cross section.

As we pointed out in an earlier publication,[1] the seven-state calculation based on V_{B1} produces an excitation cross section that is shifted a bit to the high-energy side of the experimental curve and which, at its maximum, exceeds the measured value by a factor of 6. However, apart from this small energy shift and large scale difference, the

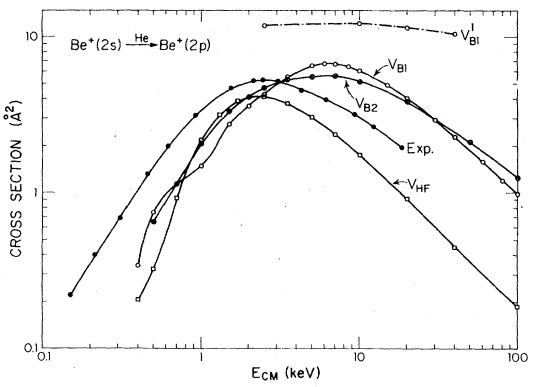

FIG. 3. Cross sections predicted for $2s \rightarrow 2p$ excitation of Be^{+} in collisions with He, as functions of center-of-mass energy $E_{\text{c.m.}}$, by calculations based on the Bottcher potentials V_{B1}, V_{B2} (marked ○ and ⊗, respectively) and V_{B1}^{l} (marked ○ – • – ○), and the Hartree-Fock frozen-core potential V_{HF} (marked □). The curve denoted Exp. (points marked ●) is the experimental result of Andersen *et al.*[3]

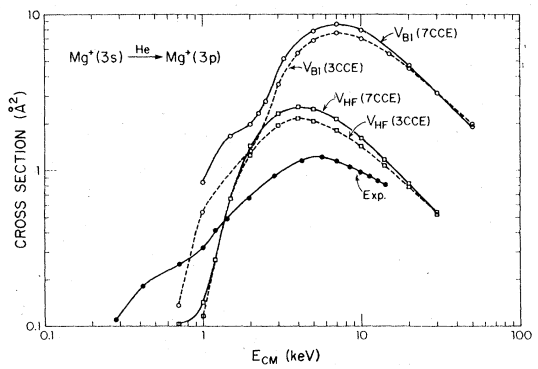

FIG. 4. Cross sections predicted for $3s \rightarrow 3p$ excitation of Mg^{+} in collisions with He as functions of center of mass energy $E_{\text{c.m.}}$ from seven-state (full line) and three-state (dashed line) calculations on the basis of model potentials V_{B1} (marked ○) and V_{HF} (marked □). The curve denoted Exp. (points marked ●) is the expermental result of Andersen *et al.* (Ref. 3).

shape of the theoretical cross-section curve is remarkably similar to the experimental emission curve. We note that according to the low-energy experiments of Ovchinnikov *et al.*[7] the cross sections in the medium-energy range may be somewhat larger than those measured by Andersen *et al.*

It can be seen that the three-state close-coupling approximation to the $3s \rightarrow 3p$ cross section falls considerably below the seven-state curve at low energy and slightly above it at high energy, indicating that the effect of the sparsely populated $3d$ and $4s$ states is to enhance the $3p$ population at low energy and to deplete it as the energy rises. This same trend is apparent in the three-state and seven-state calculations based on the Hartree-Fock frozen-core potential V_{HF}. The excitation cross sections computed for this potential agree much better with experiment throughout the medium- and high-energy range than do the predictions based on V_{B1}: the ratio of the V_{HF} to experimental cross section is less than 2 from $E_{\mathrm{c.m.}} = 1$ to 20 keV, cf. the corresponding and similar results for the $2s \rightarrow 2p$ excitation in Be^+-He collisions reported in Sec. III A. Here, as it was in the case Be^+-He, the cross-section maximum for V_{HF} occurs at a lower energy than that for V_{B1}. In the present case the maximum for V_{HF} is located at $E_{\mathrm{c.m.}} \approx 40$ keV, whereas the measured value is $E_{\mathrm{c.m.}} \approx 50$ keV. At low energy, all of the theoretical cross sections fall off too rapidly with diminishing energy. This is a characteristic common to most impact-parameter calculations based on expansions in terms of *atomic* states.

In Fig. 5 we compare on a linear-log scale the

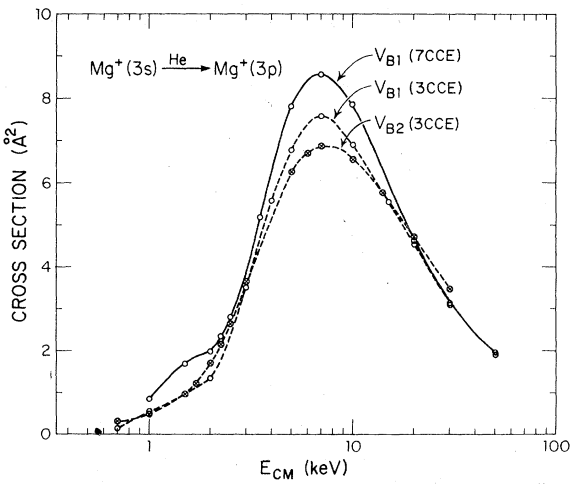

FIG. 5. Comparison of V_{B1} and V_{B2} predictions for Mg^+ $3s \rightarrow 3p$ excitation cross sections in collisions with He. Symbols for V_{B1} results are as given in the caption to Fig. 4; the three-state V_{B2} results are labeled ⊗.

$3s \rightarrow 3p$ cross sections predicted by the two model potentials V_{B1} and V_{B2}. Because the three-state and seven-state results were so similar for V_{B1} we chose only to perform three-state calculations for V_{B2}. The maximum value of the cross section is reduced by about 10% when the potential changes from V_{B1} to V_{B2}. This is accompanied by slight increases on the wings of the bell-shaped curve of the excitation cross section. These trends are similar to those discussed above for Be^+-He collisions and here, as before, we conclude that inclusion of the cross-polarization interaction does not substantially alter the comparison between theory and experiment.

Finally, in Fig. 6 we present predictions for the $3s \rightarrow 3d$ and $3s \rightarrow 4s$ excitation cross sections based on the two model potentials V_{B1} and V_{HF} and on six- and seven-state close-coupling approximations, respectively, to the scattering equations. Also shown in this figure are the experimental 3^2P-3^2D and 3^2P-4^2S MgII emission cross sections measured by Andersen *et al.*[3] These do not include cascade corrections which Andersen *et al.*[26] estimate to be less than 30% at $E_{\mathrm{c.m.}} = 6$ keV.

The $3s \rightarrow 3d$ cross section predicted by V_{B1} peaks at the same energy ($E_{\mathrm{c.m.}} \approx 15$ keV) that an experi-

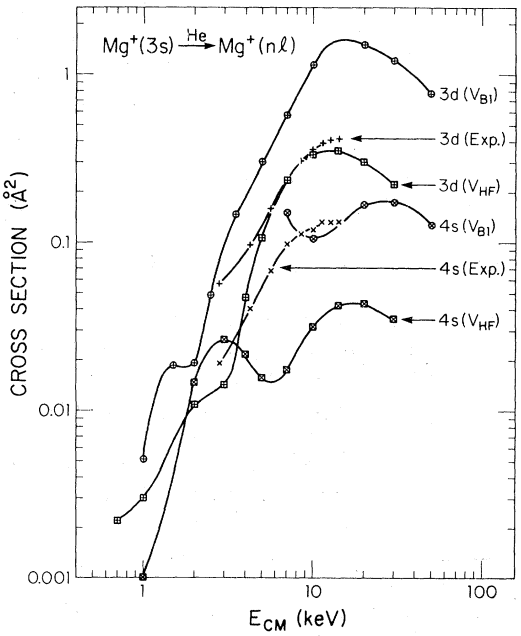

FIG. 6. Cross sections predicted for $3s \rightarrow 3d$ and $3s \rightarrow 4s$ excitations of Mg^+ in collisions with He, as functions of center-of-mass energy $E_{\mathrm{c.m.}}$, by calculations based on model potentials V_{B1} ($3d$ excitation marked ⊕, $4s$ excitation marked ⊗) and V_{HF} ($3d$ excitation marked ⊞, $4s$ excitation marked ⊠). The curves labeled Exp. are the experimental results of Andersen *et al.* (Ref. 3) for $3d$ excitation (marked +) and $4s$ excitation (marked ×).

mental maximum is indicated. However, the peak value of the theoretical cross section is four times greater than that measured. The magnitude of the $3s \rightarrow 3d$ cross section based on V_{HF} agrees very well with experiment.

Although the magnitude of the $3s \rightarrow 4s$ cross section obtained from V_{B1} is very nearly equal to the experimental value at $E_{c.m.} = 15$ keV, the limited range of energies included in our calculations precludes the possibility of making a more thorough comparison. For energies in excess of about 4 keV, the V_{HF} predictions for this transition are considerably smaller, but of the same order of magnitude as the V_{B1} and experimental values. At lower energies there is closer agreement between the V_{HF} and experimental cross sections. Corrections for cascading will improve the agreement in the medium-energy range between experiment and these Hartree-Fock predictions.

The theoretical cross sections exhibit undulations, more pronounced for the $3s \rightarrow 4s$ than for the $3s \rightarrow 3d$ transition, for which there is no experimental confirmation. However, because the strongly coupled $4p$ states were not included in the present calculations we are reluctant to place much confidence in such specific features of our estimates for the $3d$ and $4s$ excitation cross sections. It is nevertheless encouraging that these calculations successfully account for the relative magnitudes of the $3p$, $3d$, and $4s$ cross sections.

C. Be^+-Ne

We turn now to the collisional excitation of Be^+ (and later Mg^+) by target Ne atoms. Here the picture that emerges from the predictions of the various model potentials is rather different from that for He.

Estimates of cross sections for the $2s \rightarrow 2p$ excitation of Be^+ are shown in Fig. 7. These are the results of three-state calculations based on the model potentials V_{B1}, V_{B2}, and V_{HF}. The experimental emission cross section for the 2^2S-2^2P BeII multiplet shown in this figure, has not been corrected for cascading. The most striking feature is the great similarity of the three model potential curves. The V_{B1} and V_{B2} results are scarcely distinguishable over the entire energy range. Indeed it hardly could be otherwise considering the near equality of the matrix elements [see Fig. 2(c)] of these two potentials for the relevant values of R. All three model potentials predict that at low energies the cross section is a rapidly increasing function of energy with a slope very nearly equal to that observed experimentally. Even at higher energies, beyond the cross-section maximum at about $E_{c.m.}^{expt} = 12$ keV, the values predicted by V_{HF} continue to remain within (60–70)% of those of V_{B1} and V_{B2}. This stands in stark contrast to what we found for Be^+-He collisions.

The position of the maximum of the cross section (at $E_{c.m.} \approx 14$ keV) and of its magnitude (≈ 5 Å^2) predicted by V_{HF} agree slightly better with the experimental values ($\sigma_{max} \approx 3$ Å^2 at $E_{c.m.} \approx 12$ keV) than do those generated by V_{B1}/V_{B2}. All three model potentials predict that the maximum will be followed by a broad region, extending from about 10 to 100 keV, over which the cross section varies only slightly. However, the measurements of Andersen *et al.* reveal a much more rapid decrease of the cross section with rising energy, and the introduction of cascade corrections would magnify this difference between the energy dependencies of the theoretical and experimental cross sections.

D. Mg^+-Ne

Included in Fig. 8 are $3s \rightarrow 3p$ excitation cross sections for Mg^+-Ne obtained from three and seven-state close-coupling calculations, based on the model potentials V_{HF} and V_{B1}, as well as the experimental emission cross section for the 3^2S-3^2P MgII multiplet, corrected for the observed cascades from the 3^2D and 4^2S levels. Here, as with the Be^+-Ne collisions of the preceding subsection, predictions based on the two model potentials are very much alike. The theoretical cross sections based on V_{HF} are smaller than those of V_{B1}, but agree to within 30% over the entire energy range investigated. All of the theoretical cross sections are weakly undulatory functions of

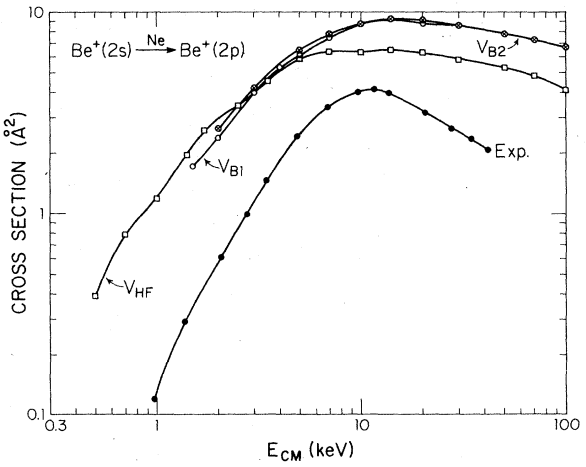

FIG. 7. Cross sections predicted for $2s \rightarrow 2p$ excitation of Be^+ in collisions with Ne, as functions of center-of-mass energy $E_{c.m.}$, by calculations based on model potentials, V_{B1}, V_{B2}, and V_{HF}. Also shown are the experimental results of Andersen *et al.* (Ref. 3) (symbols as in Fig. 3 for $Be^+ - He$ collisions).

energy. Inclusion of the $3d$ and $4s$ states produces increases in the $3s \rightarrow 3p$ cross sections at low energies which are substantially greater than those we found for Mg^+-He collisions, cf. Fig. 4. At high energies, introduction of the $3d$ and $4s$ states slightly reduces the cross sections for the $3s \rightarrow 3p$ excitation.

All in all the agreement with experiment is not very good. Although the position of the cross-section maximum is predicted fairly accurately, the theoretical estimates of the size of the cross section are about an order of magnitude too large. Furthermore, the halfwidths of the calculated cross-section maxima are much too big, and there is no experimental evidence for the predicted undulations.

The effect of the cross-polarization potential V_{ec} is displayed separately in Fig. 9 where we compare three-state calculations for V_{B2} and V_{B1}, along with the seven-state results for V_{B1}. Although V_{ec} shifts the locations of the undulations it does not produce an overall effect comparable to what was found for the He target; cf. Fig. 5.

Finally, in Fig. 10 we present the excitation cross sections for the $3s \rightarrow 3d$ and $3s \rightarrow 4s$ transitions. As in the case of the $3s \rightarrow 3p$ transition both model potentials produce qualitatively similar results. Both sets of cross sections rise rapidly with increasing energy. The $3s \rightarrow 3d$ cross sections are very weakly structured whereas the $3s \rightarrow 4s$ curves are grossly undulatory. Again, the magnitudes of the predicted cross sections are considerably larger than the measured emission cross

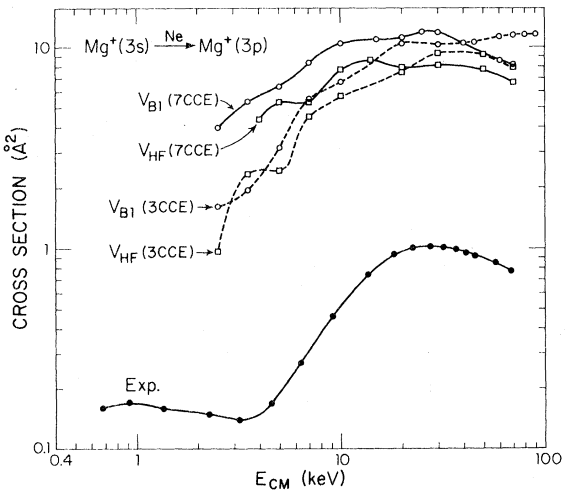

FIG. 8. Cross sections predicted for $3s \rightarrow 3p$ excitation of Mg^+ in collisions with Ne, as functions of center-of-mass energy $E_{c.m.}$, by calculations based on the model potentials V_{B1} and V_{HF}. Also shown are the experimental results of Andersen *et al.* (Ref. 3) (symbols as in Fig. 4 for Mg^+-He collisions).

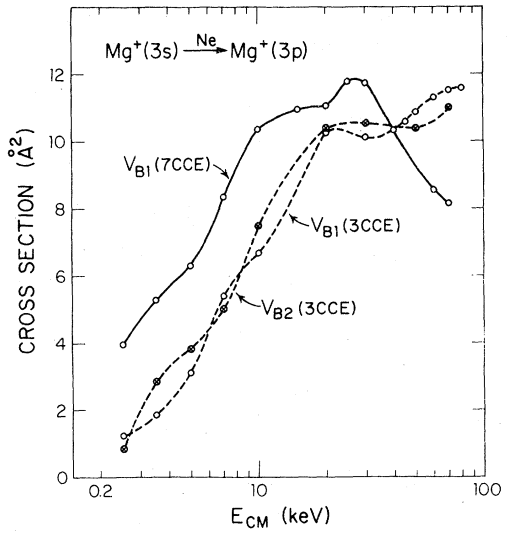

FIG. 9. Comparison of V_{B1} and V_{B2} predictions for Mg^+ $3s \rightarrow 3p$ excitation cross sections in collision with Ne (symbols as in Figs. 4 and 5 for Mg^+-He collisions).

sections for the 3^2P-3^2D and 3^2P-4^2S Mg II multiplets, especially at high energies. The predictions of the Hartree-Fock frozen-core potential are only slightly better than those of the Bottcher potential. The theory is successful in predicting that the ratio of the $3s \rightarrow 3d$ and $3s \rightarrow 4s$ cross sections diminishes as the energy falls. Finally, there is some evidence of structure in the experimental $4s$ emission

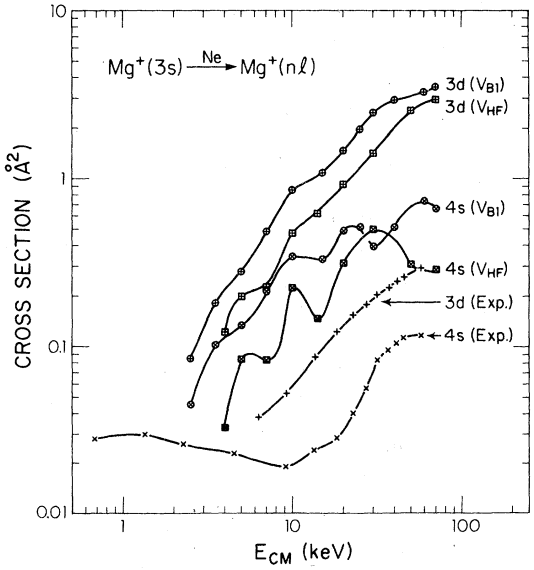

FIG. 10. Cross sections predicted for the $3s \rightarrow 3d$ and $3s \rightarrow 4s$ excitations of Mg^+ in collisions with Ne, as functions of center-of-mass energy $E_{c.m.}$, by computations based on model potentials V_{B1} and V_{HF}. Shown also are the experimental results of Andersen *et al.* (Ref. 3) (symbols as in Fig. 6 for Mg^+-He collisions).

curve, although nothing so dramatic as that predicted by either of the two model potentials.

IV. POLARIZATION OF RESONANCE LINE EMISSION

The quantity measured in the experiments of Andersen *et al.*[3] is the spectrum of the radiation emitted from the products of collisions between beam and target atoms. More specifically, they measure $I_{\parallel}$ and $I_{\perp}$, the photon-emission intensities polarized parallel and perpendicular to the direction of the ion beam and emerging at right angles from the beam axis. The polarization of this light, defined by the formula

$$P = [(I_{\parallel} - I_{\perp})/(I_{\parallel} + I_{\perp})]100(\%) , \quad (27)$$

can be expressed in terms of the cross sections σ_{nlm} by relationships which depend upon the degrees of resolution of the fine and hyperfine structures of the spectral lines.[27] Of special interest to us here are the spectra associated with radiative decay of the 2^2P and 3^2P states of Be^+ and Mg^+, respectively.

The fine structure of the BeII emission is unresolved and, although the nuclear spin is different from zero ($I=\frac{3}{2}$ for ^{9}Be), effects due to hyperfine structure appear to be small enough to be ignored.[3] Therefore, the polarization of the cascade-corrected Be II resonance line is related by the formula[28]

$$P_{nhfs}(2^2S\text{-}2^2P) = [3(\sigma_0 - \sigma_1)/(7\sigma_0 + 11\sigma_1)]100(\%) \quad (28)$$

to the excitation cross sections σ_0 and σ_1 for the $m=0$ and $m=1$ (or -1) magnetic substates of the 2^2P term. Here *nhfs* denotes "neglect of or no hyperfine structure." The effects of hyperfine structure can be taken into account if necessary by applying to P_{nhfs}, given by Eq. (28), a correction factor[28,29] which for $I=\frac{3}{2}$ is very nearly independent of impact energy and lies in the range from 0.27 to 1; the value 0.27 applies when the hyperfine structure is well separated compared to the natural linewidth.

In the case of MgII, the fine structure of the resonance line is resolved. Because the nuclear spin of ^{24}Mg is zero, there is no hyperfine structure. Therefore, the polarization of the cascade-corrected resonance line should be compared with theoretical predictions based on the formula[28]

$$P_{nhfs}(3^2S_{1/2}\text{-}3^2P_{3/2}) = [3(\sigma_0 - \sigma_1)/(5\sigma_0 + 7\sigma_1)]100(\%) . \quad (29)$$

A. Be^+-Mg^+-He

Shown in Fig. 11 are polarizations of the 2^2S-2^2P BeII multiplet, for collisions of Be^+ with He, using Eq. (28) and cross sections calculated from the model potentials V_{B1}, V_{B1}^1, V_{B2}, and V_{HF}. Also included in this figure is the polarization measured by Andersen *et al.*[3] (cascade corrections judged to be of no importance) for this same system. The predictions of V_{B1} and V_{B2} are fairly much the same over most of the energy range but the V_{B1} curve has more structure. The polarization predicted by V_{HF} exhibits a pronounced maximum-minimum structure with a deep dip at low energy.

We previously analyzed the oscillatory character of this polarization and found[1] that it arose from depletion of the $2p_0$ channel at an energy equal to about one-fourth of that at which the $2p_0$ cross section reaches its maximum value; this energy is somewhat less than that associated with the maximum of the total $2s \rightarrow 2p$ cross section. To first order in perturbation theory this effect can be attributed to interference and therefore described in terms of a Massey-type criterion with a ratio of approximately 2:1 for the impact velocities of the $2p_0$ maximum and the polarization minimum.

Although the magnitudes of the oscillations are clearly in error, the simple model potential V_{HF} predicts the overall behavior of the experimentally observed polarization surprisingly well. Hyperfine effects would reduce the difference between theory and experiment.

Theoretical estimates [using Eq. (29)] together with Andersen's experimental measurement of the polarization of the 3^2S-3^2P MgII multiplet for Mg^+-He collisions are shown in Fig. 12. The experimental polarization has not been corrected for cascading. Although we know that this correction

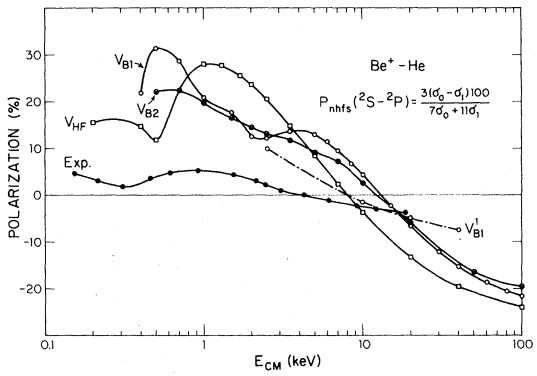

FIG. 11. Polarization of impact radiation predicted for the Be II 2^2S-2^2P resonance multiplet (unresolved fine structure) in Be^+-He collisions, neglecting hyperfine structure (P_{nhfs}). The results are based upon the four model potentials listed in the caption to Fig. 3, and the same symbols are used here as there. The experimental results are those of Andersen *et al.* (Ref. 3).

would decrease the polarization slightly for $E_{c.m.} > 10$ keV, the changes are not very important even at significantly greater energies.[1] Again V_{B1} and V_{B2} produce very similar results. The V_{HF} predictions (for three- and seven-state calculations) are shifted to lower energy (compare the corresponding shift of the total cross section shown in Fig. 4) and show a much more pronounced maximum-minimum structure. As in the case of Be^+-He, the Hartree-Fock electrostatic potential V_{HF} leads to much better agreement with experiment than either V_{B1} or V_{B2}.

B. Be^+-Mg^+-Ne

Shown in Figs. 13 and 14 are the polarizations of the Be II and Mg II resonance lines associated with collisions of Be^+ and Mg^+ with target Ne atoms. Unlike the situation with He, the predictions of the model potentials V_{B1}, V_{B2}, and V_{HF} all are very similar. Each predicts that the polarization will decrease with rising energy and exhibit weak undulations even at energies well above the cross-section maximum. The theoretical estimates of the rates of decrease are fairly good at high energy, but the experimental curves betray no evidence of the predicted undulations. Moreover, the theoretical curves do not show the pronounced maximum-minimum structure that we found in the case of He; must noticeable is the absence of a low-energy dip. On the other hand, each of the experimental polarizations shows a well-developed maximum and for Mg^+-Ne there is even a broad low-energy dip. Actually these disparities between experiment and theory may not be so great as they appear. According to our V_{HF} calculations the maxima for σ_0 (which are broader and more poorly defined for Ne than He) occur at $E_{c.m.} = 1.7$ keV for Be^+-Ne and at $E_{c.m.} = 10$ keV for Mg^+-Ne. According to the Massey criterion cited earlier, $E_{max} \sim \frac{1}{4} E_{min}$ and so the polarization minima are expected to appear at the fairly low energies, $E_{c.m.} \approx 0.4$ and 2.5 keV, respectively, which lie beyond the lower limit of our calculations.

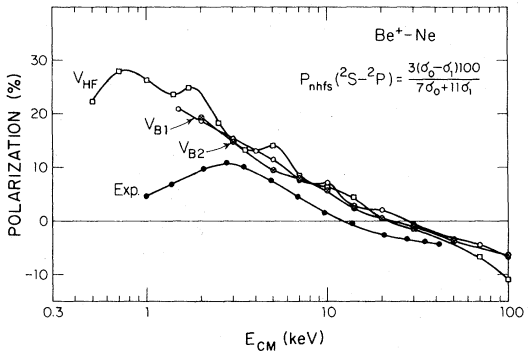

FIG. 13. Polarization of impact radiation predicted for the Be II 2^2S-2^2P resonance multiplet (unresolved fine structure) in Be^+-Ne collisions, neglecting hyperfine structure (P_{nhfs}), by calculations based on the model potentials V_{B1}, V_{B2}, and V_{HF}. The experimental results are those of Andersen *et al.* (Ref. 3) (symbols as in Fig. 3).

V. SUMMARY

We have found that the two Bottcher potentials V_{B1} and V_{B2} produce very similar estimates for the ion-excitation total cross sections and for the polarization of impact radiation in Be^+-Mg^+-He-

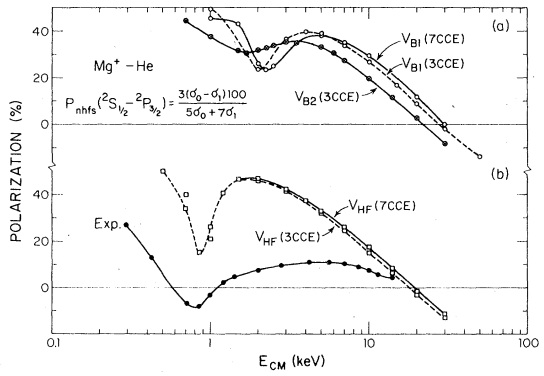

FIG. 12. Polarization of impact radiation predicted for the Mg II $3^2S_{1/2}$-$3P_{3/2}$ multiplet component in Mg^+ – He collisions (no hyperfine structure, P_{nhfs}) from close-coupling calculations based upon (a) V_{B1} and V_{B2}, and (b) V_{HF}. The experimental results of Andersen *et al.* (Ref. 3) are shown in (b). Symbols are as in Fig. 4; the three-state V_{B2} results are labeled ⊗.

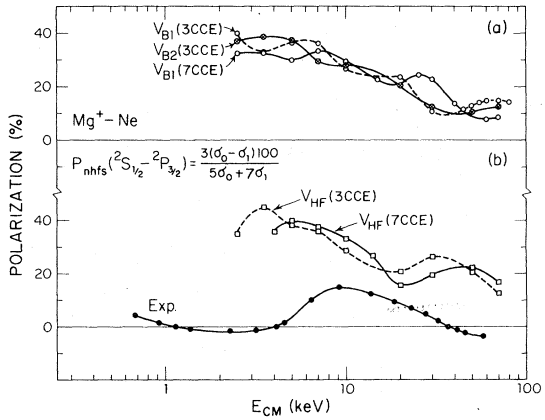

FIG. 14. Polarization of impact radiation predicted for the Mg II $3^2S_{1/2}$-$3^3P_{3/2}$ multiplet component in Mg^+ – Ne collisions (no hyperfine structure, P_{nhfs}) from close-coupling calculations based upon (a) V_{B1} and V_{B2}, and (b) V_{HF}. The experimental results of Andersen *et al.* (Ref. 3) are shown in (b). Symbols are as in Fig. 4; the three-state V_{B2} results are labeled ⊗.

Ne collisions. These similarities are especially pronounced when Ne is the target gas. Therefore, we conclude that the cross-polarization interaction V_{ec}, which distinguishes V_{B2} from V_{B1}, plays an inconsequential role in the processes considered here.

Predictions based on the Hartree-Fock frozen-core electrostatic potential V_{HF} agree better with experiment than do those based on V_{B1}/V_{B2}. Indeed, for target He atoms the similarities between measurements and theoretical estimates based on V_{HF} are most encouraging. In the case of Ne, the theoretical predictions based on the three potentials are very much the same and yield cross-section estimates that are too large by almost an order of magnitude. This pattern closely resembles that which we (and other investigators[14-17] as well) have found in studies of H–He-Ne collisions based on the V_{HF} potential. These findings also are consistent with our previously reported calculations[4] (and the recent experimental results[30]) for Li–He-Ne where predictions based on the Bottcher and Hartree-Fock potentials were very similar for the Ne target but differed considerably in the case of He. There can be little doubt that the static Hartree-Fock potential V_{HF} for Ne is too strong; some authors have invoked scaling laws[15] to compensate for this tendency of the Hartree-Fock model to overestimate the magnitudes of the cross sections for collisions with Ne.

Our numerical results provide strong empirical evidence of the superiority of V_{HF} over V_{B1}/V_{B2}. It may be, that for the high-impact velocities considered here, interactions associated with distortions of the rare-gas charge distributions are significantly overestimated by the static approximations V_e, V_q, and V_{ec}. It is also remarkable that V_{HF}, an exclusively attractive potential which is totally devoid of Pauli exclusion interactions, should be so successful in reproducing the experimental results. In this context we draw attention to our calculations[4] for the systems Li–He-Ne where strikingly similar cross sections and polarizations were predicted by V_{HF} (less so by V_{B1} and V_{B2}), on the one hand, and on the other by the Baylis potential U_B, which incorporates a strongly repulsive short-range pseudopotential to represent the Pauli exclusion interaction.

This study, as well as our other recent investigations of the dependence of scattering-theory calculations on the choice of model potentials, serves to emphasize the intrinsic limitations of the model-potential approach and to argue for the development of a more-self-consistent less-empirical theory. We currently are engaged in constructing a theory designed to satisfy these demands.

ACKNOWLEDGMENTS

This research was supported in part by the NSF. One of us (S.E.N.) wishes to acknowledge a grant from the Danish Natural Science Research Council and to express his gratitude for the hospitality extended to him during his visit to the University of Minnesota.

[1]S. E. Nielsen and J. S. Dahler, J. Phys. B 9, 1383 (1976).
[2]C. Bottcher, A. Dalgarno, and E. L. Wright, Phys. Rev. A 7, 1606 (1973).
[3]N. Andersen, T. Andersen, and K. Jensen, J. Phys. B 9, 1373 (1976).
[4]J. Manique, S. E. Nielsen, and J. S. Dahler, J. Phys. B (to be published).
[5]W. E. Baylis, J. Chem. Phys. 51, 2665 (1969).
[6]C. Bottcher, J. Phys. B 4, 1140 (1971).
[7]V. L. Ovchinnikov, O. B. Sphenik, and I. P. Zapesochnyi, Zh. Tekl. Fiz. 44, 612 (1974) [Sov. Phys. Tech. Phys. 19, 382 (1974)].
[8]J. Fayeton, N. Andersen, and M. Barat, J. Phys. B 9, L149 (1976).
[9]J. Morgan, J. Geddes, and H. B. Gilbody, J. Phys. B 6, 2118 (1973). This experimental paper includes a summary and critical discussion of the various calculations for H^+-H collisions.
[10]C. Chang and D. Rapp, J. Chem. Phys. 59, 1266 (1973).
[11]D. Rapp and C. Chang, J. Chem. Phys. 59, 1276 (1973).
[12]C. F. Melius and W. A. Goddard III, Phys. Rev. A 10, 1541 (1974).
[13]P. Habitz and W. H. E. Schwarz, Chem. Phys. Lett. 34, 248 (1975).
[14]M. R. Flannery, J. Phys. B 2, 913 (1969).
[15]H. Levy II, Phys. Rev. 187, 136 (1969).
[16]K. L. Bell, A. E. Kingston, and T. G. Winter, J. Phys. B 7, 1339 (1974).
[17]H. Levy II. Phys. Rev. A 1, 750 (1970).
[18]K. L. Bell, A. E. Kingston, and T. G. Winter, J. Phys. B 9, L279 (1976).
[19]C. Benoit and J. P. Gauyacq, J. Phys. B 9, L391 (1976).
[20]C. Bottcher, K. K. Docken, and A. Dalgarno, J. Phys. B 8, 1756 (1975).
[21]C. Bottcher and M. Oppenheimer, J. Phys. B 5, 492 (1972).
[22]R. V. Krotkov, F. W. Byron, J. A. Madeiros, and K. H. Yang, Phys. Rev. A 5, 2078 (1972).
[23]E. Clementi, IBM J. Res. Dev. 9, 2 (1965).
[24]K. Wahlstrand, R. W. Numrich, J. S. Dahler, and S. E. Nielsen, J. Phys. B (to be published).
[25]A. Messiah, *Quantum Mechanics* (Interscience, New

York, 1962), Appendix CIV.
[26]N. Andersen, K. Jensen, J. Jepsen, J. Melskens, and E. Veje, Z. Phys. A 273, 1 (1975).
[27]U. Fano and J. Macek, Rev. Mod. Phys. 45, 553 (1973).
[28]D. R. Flower and M. J. Seaton, Proc. Phys. Soc. Lond. 91, 59 (1967).
[29]D. Leep and A. Gallagher, Phys. Rev. A 10, 1082 (1974).
[30]J. Østgaard Olsen, N. Andersen, and T. Andersen, J. Phys. B (to be published).